metals

MDPI

Article

Stability, Electronic Structure, and Dehydrogenation Properties of Pristine and Doped 2D MgH_2 by the First Principles Study

Xu Gong and Xiaohong Shao *

College of Science, Beijing University of Chemical Technology, Beijing 100029, China; 2016200908@mail.buct.edu.cn

* Correspondence: shaoxh@mail.buct.edu.cn; Tel.: +86-10-64433867

Received: 30 May 2018; Accepted: 18 June 2018; Published: 25 June 2018

Abstract: Based on first principles calculations, we theoretically predict the new two-dimensional (2D) MgH_2. The thermodynamic stability, partial density of states, electron localization function, and Bader charge of pure and the transition metal (Ti, V, and Mn) doped 2D MgH_2 are investigated. The results show that all the systems are dynamically stable, and the dehydrogenation properties indicate that the decomposition temperature can be reduced by introducing the transition metal, and the Mn doped system exhibits good performance for better hydrogen storage and dehydrogenation kinetics.

Keywords: 2D MgH_2; hydrogen storage; first principles; dehydrogenation kinetics

1. Introduction

Hydrogen energy is considered to be the most promising alternative because it is lightweight, environmentally friendly, highly efficient, renewable, and abundant on earth. However, the storage limits the application of hydrogen. Metal hydrides are considered as the most promising materials for hydrogen storage and have been widely investigated in the past decades [1]. Among them, magnesium-based alloys and magnesium hydrides can achieve the hydrogen storage capacity of 7.6 wt % [2–8]. However, the high thermodynamic stability (the heat of formation is around −75.99 kJ/mol·H_2), high desorption temperatures (above 573 K), and slow dehydrogenation kinetics seriously limit the practical applications [3,9,10]. Therefore, it is always a central task to design new materials or adopt efficient strategies for achieving lower desorption temperatures and good dehydrogenation performances.

Previous studies show that the bonding nature of MgH_2 is a mixture of strong ionic and weak covalent bonding [11], and weakening the interactions may be an effective strategy to improve dehydrogenation performance. It has been reported that doping with transition metal elements or their oxides mixtures with MgH_2 can effectively reduce its stability and improve the hydrogen desorption thermodynamics [3,12–17]. Oelerich [15] et al. have reported that MgH_2 milled with Fe_3O_4, V_2O_5, Mn_2O_3, or Cr_2O_3, etc. can accelerate the hydrogen desorption kinetics. Shang [3] et al. have studied the hydrogen storage performance of (MgH_2 + M) systems (M = Al, Ti, Fe, Ni, Cu, and Nb) experimentally and theoretically, and they found that MgH_2 mixed with those metals can reduce the stability and improve the hydrogen desorption kinetics. Nonetheless, the MgH_2 systems still have a high desorption temperature around 500 K. It is noted that the bulk MgH_2 has been extensively investigated, however, the single-layer magnesium hydrides have been largely ignored. Motivated by the above mentioned details, we focus on exploring new structures with good dehydrogenation performance in this work.

In this paper, the new two-dimensional (2D) MgH_2 structure is theoretically predicted and studied by first principles calculations. The stabilities of pure and Ti/V/Mn doped MgH_2 are discussed by the

phonon spectra and heat of formation. The calculated heat of formation for pure and Ti/V/Mn doped 2D MgH_2 are −37.57, −25.67, −18.14, and −23.90 kJ/mol·H_2, respectively, which are significantly lower than that of −75.99 kJ/mol·H_2 of bulk MgH_2. The electronic structure and hydrogen desorption kinetics results show that the predicted two-dimensional magnesium hydride are promising candidates for hydrogen storage.

2. Computational Details

The structural optimization and electronic property calculations were performed using the projector augmented plane-wave method (PAW) based on the density functional theory (DFT) in the Vienna ab initio simulation package (VASP) [18,19]. The exchange-correlation potential was approximated by generalized gradient approximation (GGA) in the Perdew-Burke-Ernzerhof (PBE) form [20,21]. To avoid the interlayer effects of the *c*-axis, the vacuum region around 15 Å was set in all the systems. The energy cutoff of 600 eV and the 9 × 9 × 1 Γ-centered Monkhorst-Pack *k*-points [22] were employed for all calculations. The atomic positions were fully relaxed and the force tolerance between each atom was less than 0.01 eV/Å for the structural optimization. The convergence criteria of 10^{-6} eV per atom was applied to be self-consistent. Meanwhile, for calculation of electronic structures, we also applied the local density approximation (LDA) [23] and HSE06 [24] was functional. The kinetic stability was discussed using the phonon spectra calculations in PHONOPY code coupled with VASP using the density functional perturbation theory (DFPT) method [25–27].

3. Results and Discussion

Figure 1 shows the fully relaxed structure of the top and side view of pure 2D MgH_2 of the hexagonal structure with space group *P-3m1* (D^3_{3d}). The primitive cell has the lattice constant of $a = b = 3.01$ Å, the Mg-H bond length of $l = 1.97$ Å, and the buckled height of $d = 1.86$ Å. The next calculations were performed for the 3 × 3 × 1 supercell of 2D MgH_2, named Mg_9H_{18}. The corresponding lattice parameters, Wyckoff [28] and atomic positions, are shown in Table 1. As is seen, there are nine Mg atoms located at 1b (Mg1), 6h (Mg2), and 2d (Mg3) sites, while the eighteen H atoms are located in three identical Wyckoff positions, i.e., 6i, as shown in Figure 1.

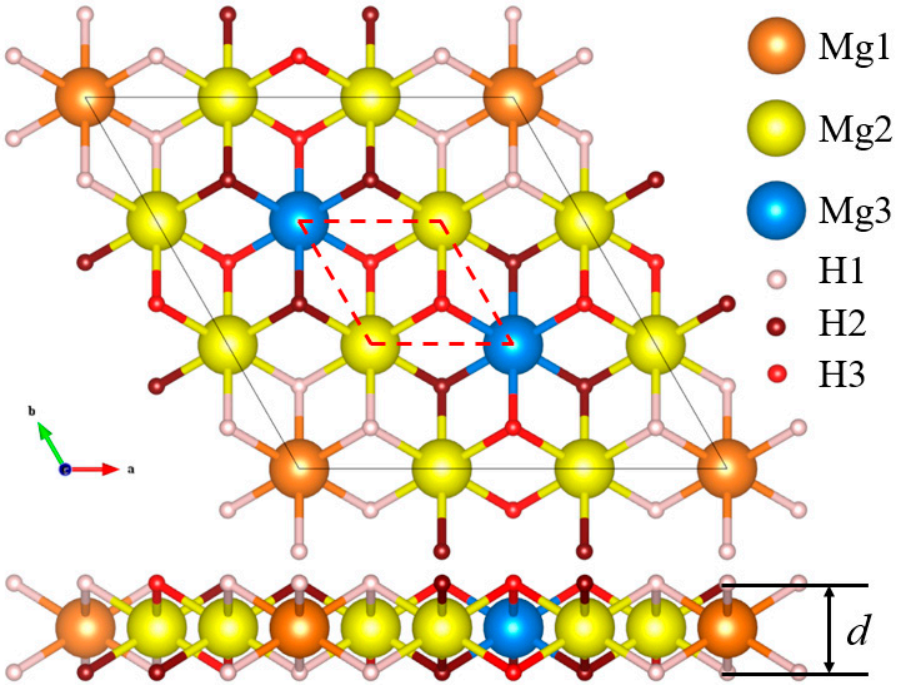

Figure 1. The relaxed unit cell of Mg_9H_{18}. The primate cell is marked with a red dashed box.

Table 1. The relaxed structural parameters and atomic positions of Mg_9H_{18}.

Lattice Parameters	Atom	Wyckoff	Atomic Positions (Fractional)		
		Positions	x	y	z
164(*P-3m1*)	Mg1	1b	0	0	0.5
$a = b = 9.033$ Å	Mg2	6h	0	0.33333	0.5
$c = 15$ Å	Mg3	2d	0.33333	0.66667	0.5
$d = 1.86$ Å	H1	6i	0.11111	0.22222	0.43783
$\alpha = \beta = 90°$	H2	6i	0.22222	0.44444	0.56217
$\gamma = 120°$	H3	6i	0.11111	0.55556	0.43783

In this work, three different Mg sites are considered as possible positions for substitution doping. Meanwhile, defects are inevitable in synthesis or processing and can usually affect their properties [29–33]. The most common types of defect are vacancy defects, so we also considered the vacancies of Mg (Mg_8H_{18}) for comparison to the doped systems. The formation energies were calculated to determine the favorable positions of doping elements of Ti/V/Mn, which is defined as $\Delta E = E_{tot}(Mg_8H_{18}X_n) - E_{tot}(Mg_9H_{18}) - n\,E_{tot}(X) + E_{tot}(Mg)$, where E_{tot} is the total energy of the system, the parameter $n = 0/1$ represents Mg vacancy, and X (X = Ti, V, and Mn) doped. The energies are listed in Table 2. It is noticed that the Mg_8H_{18} and Ti/V/Mn doped systems have positive energy, indicating that the stability of all the systems are lower than that of pure Mg_9H_{18}. In addition, for the three high symmetry sites of Mg1 (1b), Mg2 (6h), and Mg3 (2d), the ΔE are nearly identical, therefore, we assume that all the doped-sites are located at the Mg1 site in the following work. The relaxed parameters and bond lengths of Mg_9H_{18} and $Mg_8H_{18}X$ (X = Ti, V, and Mn) are listed in Table 2, and for the detailed lattice parameters, see Table A1 (Appendix A). As is seen, the bond length of Mg-H is changed, which indicates that the doped X atoms break the symmetry of the 2D MgH_2 structure.

Table 2. The energy (ΔE), the lattice parameter (a), and bond length of Mg_9H_{18}, Mg_8H_{18} and $Mg_8H_{18}X$ (X = Ti, V, and Mn).

Hydride	ΔE (eV)			Parameter	Bond Length (Å)					
	Mg1	Mg2	Mg3	a (Å)	Sub-H1	Mg2-H1	Mg2-H2	Mg2-H3	Mg3-H2	Mg3-H3
Mg_9H_{18}	0	0	0	9.033	1.972	1.972	1.972	1.972	1.972	1.972
Mg_8H_{18}	2.968	2.968	2.968	9.062	-	1.894	2.043	1.976	1.947	1.992
$Mg_8H_{18}Ti$	1.113	1.114	1.114	9.027	1.915	1.997	1.964	1.982	1.946	1.990
$Mg_8H_{18}V$	1.818	1.818	1.819	8.951	1.822	1.999	1.945	1.992	1.939	1.983
$Mg_8H_{18}Mn$	1.279	1.279	1.279	8.815	1.691	2.028	1.911	2.008	1.937	1.965

Structural stability is discussed by the phonon spectra calculations using the DFPT method, as is shown in Figure 2. Clearly, there are no imaginary frequencies in the whole Brillouin zone, indicating that all the systems are dynamically stable. Meanwhile, the heat of formation (ΔH) [7,34–36] is one of the most fundamentally thermodynamic properties. The heat of formation can be obtained directly from the equation $\Delta H = [E_{tot}(Mg_{9-n}H_{18}X_{n+m}) - (n + m)\,E_{tot}(X) - (9\text{-}n)\,E_{tot}(Mg) - 9\,E_{tot}(H_2)]/9$, where the parameters ($n = 0$, $m = 0$), ($n = 1$, $m = -1$), and ($n = 1$, $m = 0$), represent pure, Mg vacancy, and X (X = Ti, V and Mn) doped Mg_9H_{18}, respectively. The value of $E_{tot}(H_2)$ of -6.762 eV in a $10 \times 10 \times 10$ Å^3 cubic cell is very close to -6.773 eV reported in Ref. [37].

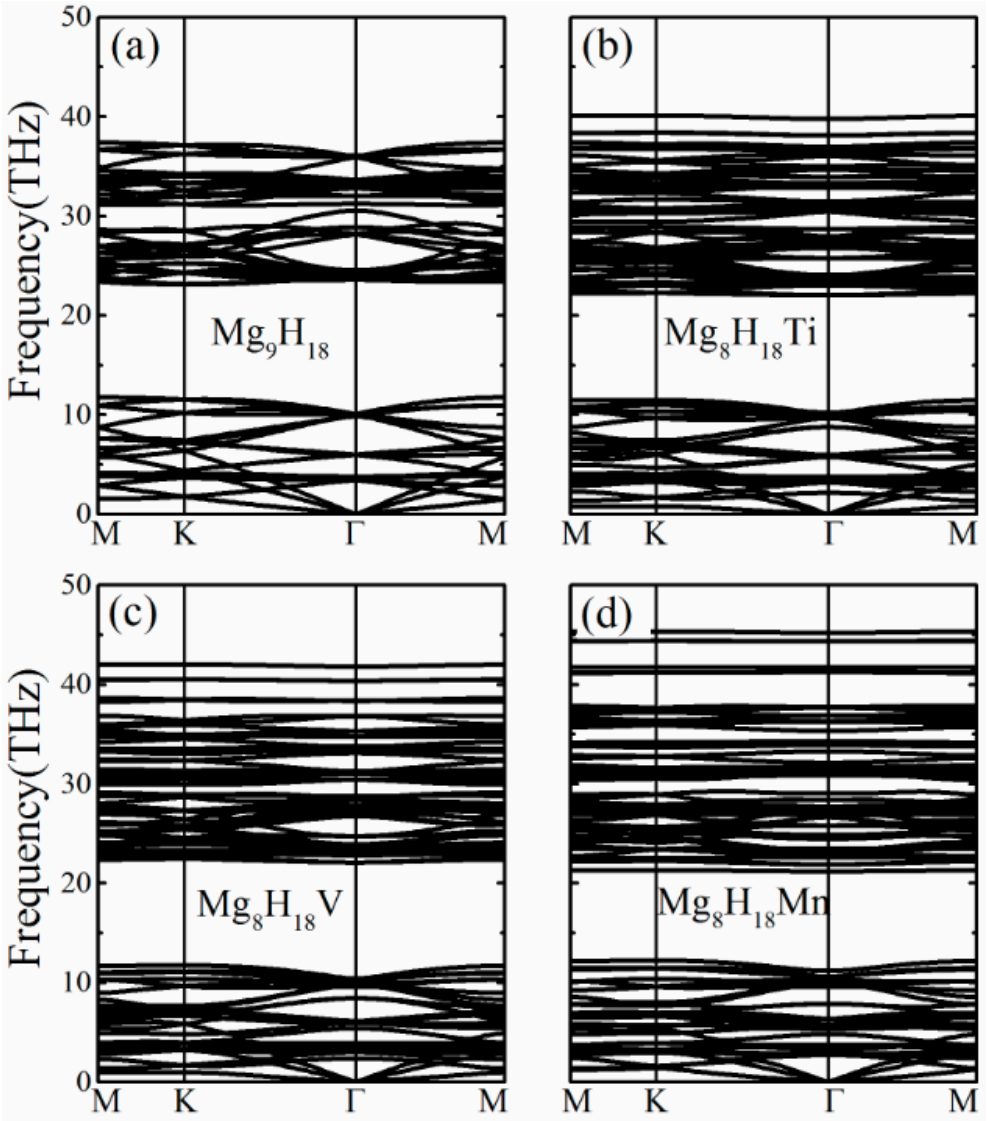

Figure 2. The phonon spectra of Mg_9H_{18} (**a**); $Mg_8H_{18}Ti$ (**b**); $Mg_8H_{18}V$ (**c**); and $Mg_8H_{18}Mn$ (**d**).

The estimated heats of formation are listed in Table 3. As is seen, the heat of formation of Mg_9H_{18}, Mg_8H_{18}, $Mg_8H_{18}Ti$, $Mg_8H_{18}V$, and $Mg_8H_{18}Mn$ are −37.57, 31.71, −25.67, −18.14, and −23.90 kJ/mol·H_2, respectively. The results show that the stability decreased for the doped 2D MgH_2, followed by $Mg_8H_{18}Ti$, $Mg_8H_{18}Mn$, and $Mg_8H_{18}V$, and Mg_8H_{18} is the most unstable. In comparison, we also obtained the heat of formation of the bulk MgH_2 of ΔH = −54.56 kJ/mol·H_2, which is close to the theoretical values −54.4 in Ref. [36] and −53.85 kJ/mol·H_2 in Ref. [38]. At the same time, we estimated the decomposition temperature according to the following relationship: $\ln \frac{P}{P_0} = \frac{\Delta H}{RT} - \frac{\Delta S}{R}$, where P, P_0, R, T, and ΔS represent the pressure, the standard pressure, the gas constant, the decomposition temperature, and the entropy change, respectively. At the standard pressure, the ΔH is defined as $\Delta H = T\Delta S$ [39,40]. For most of the dehydrogenation reactions of simple metal hydrides, the ΔS is in the range of 95 J/mol·K < $\Delta S(H_2)$ < 140 J/mol·K [41]. Consequently, the decomposition temperatures are 268 K < $T(Mg_9H_{18})$ < 396 K, 183 K < $T(Mg_8H_{18}Ti)$ < 270 K, 130 K < $T(Mg_8H_{18}V)$ < 191 K, 171 K < $T(Mg_8H_{18}Mn)$ < 252 K, which are significantly lower than that of 573~673 K of bulk MgH_2. The discussions mentioned above show that 2D MgH_2 has better dehydrogenation thermodynamic properties than that of bulk MgH_2, and doping with Ti, V, and Mn elements can reduce the stability and improve the dehydrogenation thermodynamics properties of 2D MgH_2.

Table 3. The heat of formation (ΔH), the decomposition temperature (T), Bader charge of Mg and H atoms, and the dehydrogenation energies (E_d) of Mg_9H_{18}, Mg_8H_{18}, and $Mg_8H_{18}X$ (X = Ti, V, and Mn).

Hydride	ΔH	T	Bader Charge (e)			E_d
	(kJ/mol·H_2)	(K)	Mg	X	H	(eV)
Mg_9H_{18}	−37.57	268~396	+2.000	-	−0.997	1.589
Mg_8H_{18}	31.71	-	+2.000	-	−0.886	−1.931
$Mg_8H_{18}Ti$	−25.67	183~270	+2.000	+1.825	−0.988	1.305
$Mg_8H_{18}V$	−18.14	130~191	+2.000	+1.523	−0.971	1.044
$Mg_8H_{18}Mn$	−23.90	171~252	+2.000	+0.975	−0.940	0.853

To understand the effect of Ti/V/Mn-doped 2D MgH_2 well, we analyzed the electronic structures. The band structures were obtained using PBE, LDA, and HSE06 functionals and are shown in Figure A1. It can be seen that the pure Mg_9H_{18} with the energy gap is 4.87 eV, which is smaller than the experimental values 5.16 eV [42] or 5.6 eV [43] of bulk MgH_2. For comparison, we found that the bandgaps using HSE06 functional are larger than those using PBE and LDA functionals, and the bandgaps using LDA functional are close to those of the PBE functional for pure and vacancies of Mg_9H_{18}. For the doped systems, there are few energy bands across the Fermi level due to the d orbitals of the dopants. Figure 3 shows the total and partial density of states (PDOS) of Mg_9H_{18} and Mg_8H_{18}, which are calculated using the PBE functional. We can see the stronger hybridization between H and Mg atoms near the Fermi level, which indicates the strong interaction between H and Mg atoms. For the $Mg_8H_{18}X$, the electronic structure is different from that of the pure Mg_9H_{18}, as is shown in Figure 4. We can see that the d orbitals of Ti/V/Mn are mainly located near the Fermi level in doped-2D MgH_2, and there are few H-s orbitals and states of Mg atoms at the Fermi level, which indicates that the interactions between Ti/V/Mn and H/Mg atoms are relatively weaker. Meanwhile, since the H-s orbitals are reduced at the Fermi level, the hybridization between H and Mg atoms is weaker compared to pure Mg_9H_{18}.

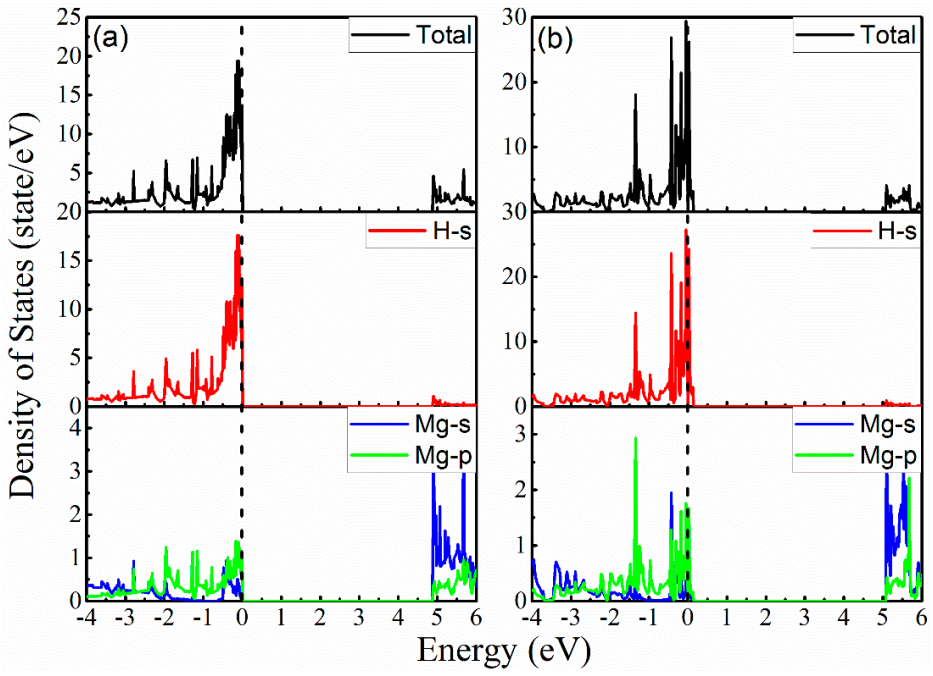

Figure 3. The total and partial densities of states of pure (**a**) and defective (**b**) Mg_9H_{18}.

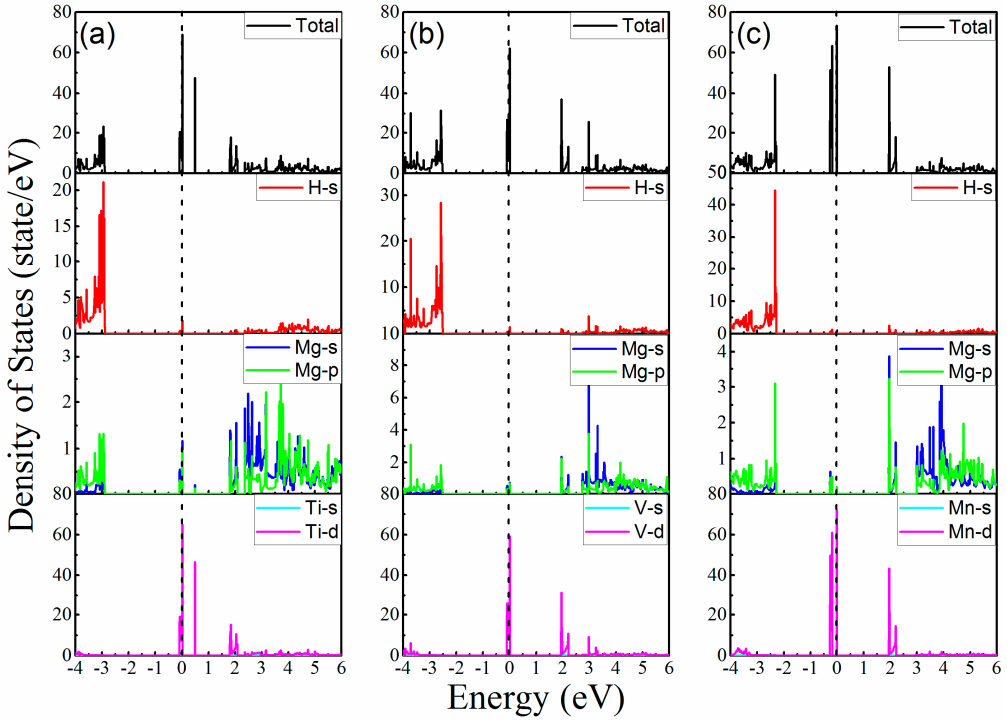

Figure 4. The total and partial densities of states of $Mg_8H_{18}Ti$ (**a**); $Mg_8H_{18}V$ (**b**); and $Mg_8H_{18}Mn$ (**c**).

In order to analyze the chemical bond of all the systems, the electron localization function (ELF) was calculated and is shown in Figure 5 with the isosurfaces of 0.6 e/Å^3. As shown in Figure 5b–f, all the systems have similar features in that the ELF values are lower between Mg and H atoms. These suggest that the ionic bonds exist between Mg and H atoms, and the Mg atoms act as the charge donor, according well with the discussions of PDOS and ELF of bulk MgH_2. The Bader charges were also calculated (see Table 3), and it can be seen that Mg atoms contributed two electrons, and H atoms acquired electrons to form anions. Meanwhile, the H atoms obtained fewer electrons due to the Mg vacancy and doping with Ti/V/Mn elements, thereby weakening the interactions between H and the metal atoms.

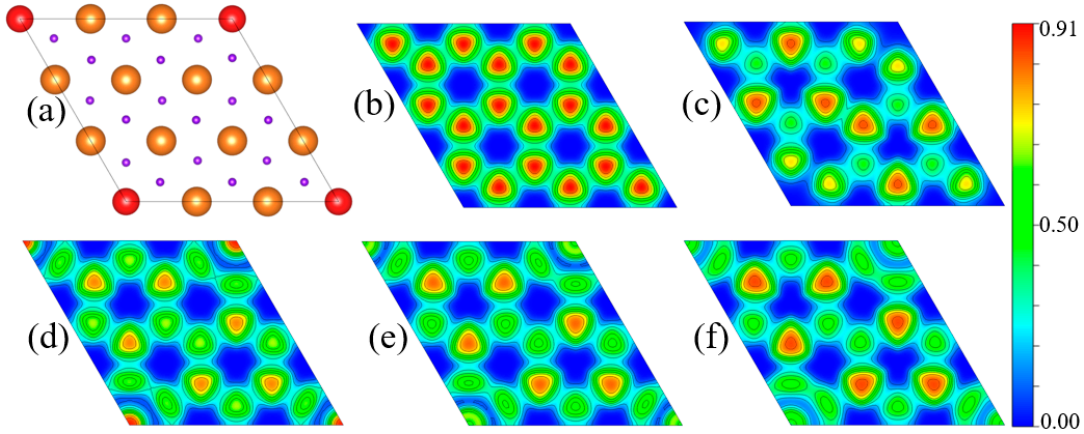

Figure 5. (**a**) Structural representation of considered systems. The big (small) ball represents Mg (H) and the red ball site is the doped site; (**b**–**f**) represent the electron localization function (ELF) of Mg_9H_{18}, Mg_8H_{18}, $Mg_8H_{18}Ti$, $Mg_8H_{18}V$, and $Mg_8H_{18}Mn$, respectively. The color bar represents the values of ELF.

As mentioned above, doping with Ti/V/Mn elements reduces the stability of 2D MgH_2 and weakens the interactions between H and metal atoms, which facilitates the release of hydrogen. To further understand the dehydrogenation behavior, the dehydrogenation energy was estimated by the formula: $E_d = E_{tot}(Mg_{9-n}H_{17}X_{n+m}) - E_{tot}(Mg_{9-n}H_{18}X_{n+m}) + 1/2\ E_{tot}(H_2)$, where ($n = 0$, $m = 0$), ($n = 1$, $m = -1$), and ($n = 1$, $m = 0$) represent the pure, Mg vacancy, and X (X = Ti, V, and Mn) doped Mg_9H_{18}, respectively. The dehydrogenation energies are listed in Table 3. The results show that the dehydrogenation energy of the Mg_8H_{18} was significantly reduced compared to the pure and doped Mg_9H_{18}, while there are high ΔE of 2.968 eV and positive ΔH of 31.71 kJ/mol·H_2, indicating that it is almost impossible to steadily occur. For doped systems, their dehydrogenation energies are significantly smaller than 1.589 eV of pure Mg_9H_{18}, especially $Mg_8H_{18}Mn$ with the dehydrogenation energy of 0.853 eV. Therefore, doping with Ti/V/Mn elements can improve the dehydrogenation thermodynamic properties of 2D MgH_2.

4. Conclusions

In summary, we theoretically predicted two-dimensional MgH_2 and studied the electronic and dehydrogenation properties of pure and Ti/VMn doped 2D MgH_2. The phonon spectra calculations indicate that all the systems are dynamically stable. The results of heat of formation suggests that Ti/V/Mn doping can reduce the thermodynamic stability, followed by $Mg_8H_{18}Ti$, $Mg_8H_{18}Mn$, and $Mg_8H_{18}V$, and Mg_8H_{18} is the most unstable. Importantly, the dehydrogenation temperatures for all the systems are significantly lower than that of bulk MgH_2 at 573~673 K. Especially, $Mg_8H_{18}Ti$ (183~270 K), $Mg_8H_{18}V$ (130~191 K), and $Mg_8H_{18}Mn$ (171~252 K) have much lower decomposition temperature than that of pure 2D MgH_2 (268~396 K), which is important for practical applications. The partial densities of states, electron localization function, and Bader charge calculation results show that Ti, V, and Mn elements can weaken the interaction between H and the metal atoms, which is favorable to dehydrogenation and better than that of the bulk MgH_2.

Author Contributions: All authors contributed equally to this work.

Acknowledgments: This work was supported by the National Natural Science Foundation of China (Grant No. 11604008) and by BUCT Fund for Disciplines Construction (Project No. XK1702).

Conflicts of Interest: The authors declare no conflicts of interest.

Appendix A

Table A1. The relaxed structure parameters of pure, vacancies, and doped Mg_9H_{18} using Perdew-Burke-Ernzerhof (PBE) and local density approximation (LDA) functionals.

Hydride	PBE				LDA			
	a (Å)	α (°)	β (°)	γ (°)	a (Å)	α (°)	β (°)	γ (°)
Mg_9H_{18}	9.033	90.0	90.0	120.0	8.894	90.0	90.0	120.0
Mg_8H_{18}	9.062	90.0	90.0	120.0	8.888	90.0	90.0	120.0
$Mg_8H_{18}Ti$	9.027	90.0	90.0	120.0	8.883	90.0	90.0	120.0
$Mg_8H_{18}V$	8.951	90.0	90.0	120.0	8.803	90.0	90.0	120.0
$Mg_8H_{18}Mn$	8.815	90.0	90.0	120.0	8.662	90.0	90.0	120.0

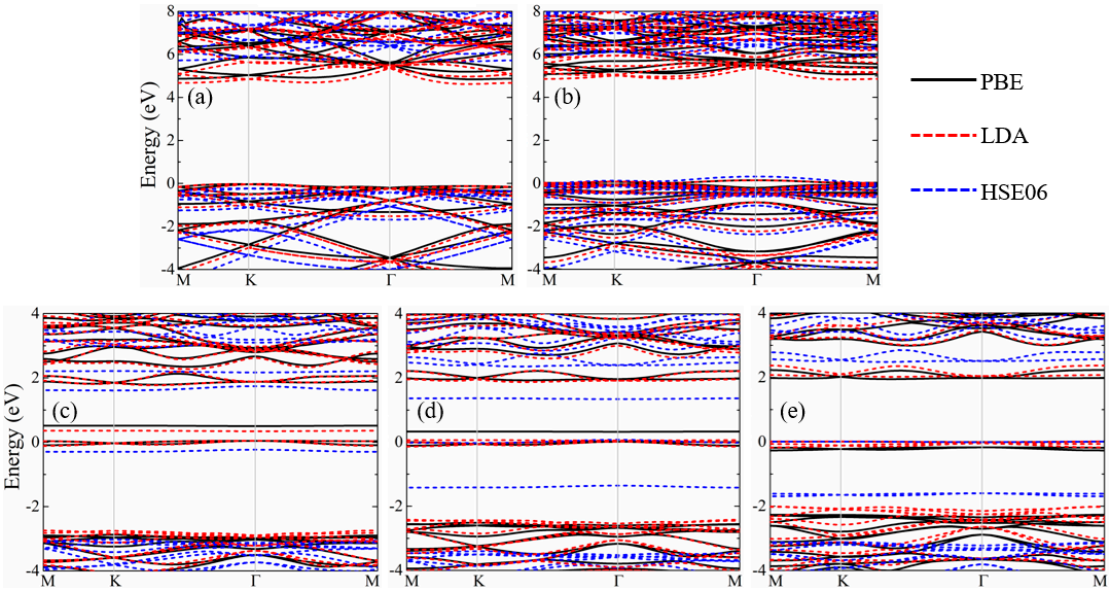

Figure A1. Band structures of Mg_9H_{18} (**a**); Mg_8H_{18} (**b**); $Mg_8H_{18}Ti$ (**c**); $Mg_8H_{18}V$ (**d**); and $Mg_8H_{18}Mn$ (**e**) calculated using PBE (black line), LDA (red dot line), and HSE06 (blue dot line) functionals, respectively.

References

1. Sakintuna, B.; Lamari-Darkrim, F.; Hirscher, M. Metal hydride materials for solid hydrogen storage: A review. *Int. J. Hydrogen Energy* **2007**, *32*, 1121–1140. [CrossRef]
2. Mohammed, Z.; Ahmed, R.; Mohammed Benali, K.; Bakhtiar ul, H.; Ahmad Radzi Mat, I.; Souraya, G.-S. First principle investigations of the physical properties of hydrogen-rich MgH_2. *Phys. Scr.* **2013**, *88*, 065704. [CrossRef]
3. Shang, C.X.; Bououdina, M.; Song, Y.; Guo, Z.X. Mechanical alloying and electronic simulations of (MgH_2 + M) systems (M = Al, Ti, Fe, Ni, Cu and Nb) for hydrogen storage. *Int. J. Hydrogen Energy* **2004**, *29*, 73–80. [CrossRef]
4. Ul Haq, B.; Kanoun, M.B.; Ahmed, R.; Bououdina, M.; Goumri-Said, S. Hybrid functional calculations of potential hydrogen storage material: Complex dimagnesium iron hydride. *Int. J. Hydrogen Energy* **2014**, *39*, 9709–9717. [CrossRef]
5. Kumar, D.; Singh, A.; Prasad Tiwari, G.; Kojima, Y.; Kain, V. Thermodynamics and kinetics of nano-engineered Mg-MgH_2 system for reversible hydrogen storage application. *Thermochim. Acta* **2017**, *652*, 103–108. [CrossRef]
6. Trivedi, D.R.; Bandyopadhyay, D. Study of adsorption and dissociation process of H_2 molecule on MgnRh clusters: A density functional investigation. *Int. J. Hydrogen Energy* **2016**, *41*, 20113–20121. [CrossRef]
7. Song, Y.; Guo, Z.X.; Yang, R. Influence of selected alloying elements on the stability of magnesium dihydride for hydrogen storage applications: A first-principles investigation. *Phys. Rev. B* **2004**, *69*, 094205. [CrossRef]
8. Vajeeston, P.; Ravindran, P.; Kjekshus, A.; Fjellvåg, H. Pressure-Induced Structural Transitions in MgH_2. *Phys. Rev. Lett.* **2002**, *89*, 175506. [CrossRef] [PubMed]
9. Kurko, S.; Matović, L.; Novaković, N.; Matović, B.; Jovanović, Z.; Mamula, B.P.; Grbović Novaković, J. Changes of hydrogen storage properties of MgH_2 induced by boron ion irradiation. *Int. J. Hydrogen Energy* **2011**, *36*, 1184–1189. [CrossRef]
10. Song, M.Y.; Kwon, S.N.; Park, H.R.; Hong, S.-H. Improvement in the hydrogen storage properties of Mg by mechanical grinding with Ni, Fe and V under H_2 atmosphere. *Int. J. Hydrogen Energy* **2011**, *36*, 13587–13594. [CrossRef]
11. Noritake, T.; Aoki, M.; Towata, S.; Seno, Y.; Hirose, Y.; Nishibori, E.; Takata, M.; Sakata, M. Chemical bonding of hydrogen in MgH_2. *Appl. Phys. Lett.* **2002**, *81*, 2008–2010. [CrossRef]

12. Liang, G.; Huot, J.; Boily, S.; Van Neste, A.; Schulz, R. Catalytic effect of transition metals on hydrogen sorption in nanocrystalline ball milled MgH_2 − Tm (Tm = Ti, V, Mn, Fe and Ni) systems. *J. Alloys Compd.* **1999**, *292*, 247–252. [CrossRef]
13. Shang, C.X.; Bououdina, M.; Guo, Z.X. Structural stability of mechanically alloyed (Mg + 10Nb) and (MgH_2 + 10Nb) powder mixtures. *J. Alloys Compd.* **2003**, *349*, 217–223. [CrossRef]
14. Rivoirard, S.; de Rango, P.; Fruchart, D.; Charbonnier, J.; Vempaire, D. Catalytic effect of additives on the hydrogen absorption properties of nano-crystalline MgH_2(X) composites. *J. Alloys Compd.* **2003**, *356*, 622–625. [CrossRef]
15. Oelerich, W.; Klassen, T.; Bormann, R. Metal oxides as catalysts for improved hydrogen sorption in nanocrystalline Mg-based materials. *J. Alloys Compd.* **2001**, *315*, 237–242. [CrossRef]
16. Aguey-Zinsou, K.F.; Ares Fernandez, J.R.; Klassen, T.; Bormann, R. Effect of Nb_2O_5 on MgH_2 properties during mechanical milling. *Int. J. Hydrogen Energy* **2007**, *32*, 2400–2407. [CrossRef]
17. Song, M.; Bobet, J.-L.; Darriet, B. Improvement in hydrogen sorption properties of Mg by reactive mechanical grinding with Cr_2O_3, Al_2O_3 and CeO_2. *J. Alloys Compd.* **2002**, *340*, 256–262. [CrossRef]
18. Kresse, G.; Furthmüller, J. Efficient Iterative Schemes for Ab Initio Total-Energy Calculations Using a Plane-Wave Basis Set. *Phys. Rev. B Condens. Matter* **1996**, *54*, 11169–11186. [CrossRef] [PubMed]
19. Kresse, G.; Joubert, D. From ultrasoft pseudopotentials to the projector augmented-wave method. *Phys. Rev. B* **1999**, *59*, 1758–1775. [CrossRef]
20. Perdew, J.P.; Burke, K.; Ernzerhof, M. Generalized Gradient Approximation Made Simple. *Phys. Rev. Lett.* **1996**, *77*, 3865–3868. [CrossRef] [PubMed]
21. Hammer, B.; Hansen, L.B.; Nørskov, J.K. Improved adsorption energetics within density-functional theory using revised Perdew-Burke-Ernzerhof functionals. *Phys. Rev. B* **1999**, *59*, 7413–7421. [CrossRef]
22. Monkhorst, H.J.; Pack, J.D. Special points for Brillouin-zone integrations. *Phys. Rev. B* **1976**, *13*, 5188–5192. [CrossRef]
23. Perdew, J.P.; Zunger, A. Self-interaction correction to density-functional approximations for many-electron systems. *Phys. Rev. B* **1981**, *23*, 5048–5079. [CrossRef]
24. Heyd, J.; Scuseria, G.E.; Ernzerhof, M. Erratum: Hybrid functionals based on a screened Coulomb potential. *J. Chem. Phys.* **2006**, *118*, 8207. [CrossRef]
25. Togo, A.; Oba, F.; Tanaka, I. First-Principles Calculations of the Ferroelastic Transition Between Rutile-Type and $CaCl_2$-Type SiO_2 at High Pressures. *Phys. Rev. B Condens. Matter* **2008**, *78*. [CrossRef]
26. Gonze, X.; Lee, C. Dynamical matrices, Born effective charges, dielectric permittivity tensors, and interatomic force constants from density-functional perturbation theory. *Phys. Rev. B* **1997**, *55*, 10355–10368. [CrossRef]
27. Baroni, S.; de Gironcoli, S.; Dal Corso, A.; Giannozzi, P. Phonons and related crystal properties from density-functional perturbation theory. *Rev. Mod. Phys.* **2001**, *73*, 515–562. [CrossRef]
28. Gu, T.; Wang, Z.; Tada, T.; Watanabe, S. First-principles simulations on bulk Ta_2O_5 and Cu/Ta_2O_5/Pt heterojunction: Electronic structures and transport properties. *J. Appl. Phys.* **2009**, *106*, 262907. [CrossRef]
29. Sun, R.; Wang, Z.; Saito, M.; Shibata, N.; Ikuhara, Y. Atomistic mechanisms of nonstoichiometry-induced twin boundary structural transformation in titanium dioxide. *Nat. Commun.* **2011**, *6*, 7120. [CrossRef] [PubMed]
30. Wang, Z.; Saito, M.; Mckenna, K.P.; Gu, L.; Tsukimoto, S.; Shluger, A.L.; Ikuhara, Y. Atom-resolved imaging of ordered defect superstructures at individual grain boundaries. *Nature* **2011**, *479*, 380–383. [CrossRef] [PubMed]
31. McKenna, K.P.; Hofer, F.; Gilks, D.; Lazarov, V.K.; Chen, C.; Wang, Z.; Ikuhara, Y. Atomic-scale structure and properties of highly stable antiphase boundary defects in Fe_3O_4. *Nat. Commun.* **2014**, *5*, 5740. [CrossRef] [PubMed]
32. Wang, Z.; Saito, M.; Mckenna, K.P.; Fukami, S.; Sato, H.; Ikeda, S.; Ohno, H.; Ikuhara, Y. Atomic-Scale Structure and Local Chemistry of CoFeB-MgO Magnetic Tunnel Junctions. *Nano Lett.* **2016**, *16*, 1530–1536. [CrossRef] [PubMed]
33. Yan, H.; Ziyu, H.; Xu, G.; Xiaohong, S. Structural, electronic and photocatalytic properties of atomic defective BiI3 monolayers. *Chem. Phys. Lett.* **2018**, *691*, 341–346. [CrossRef]
34. García, G.N.; Abriata, J.P.; Sofo, J.O. Calculation of the electronic and structural properties of cubic Mg_2NiH_4. *Phys. Rev. B* **1999**, *59*, 11746–11754. [CrossRef]

35. Chen, Y.; Dai, J.; Xie, R.; Song, Y.; Bououdina, M. First principles study of dehydrogenation properties of alkali/alkali-earth metal doped Mg_7TiH_{16}. *J. Alloys Compd.* **2017**, *728*, 1016–1022. [CrossRef]
36. Shelyapina, M.G.; Fruchart, D.; Wolfers, P. Electronic structure and stability of new FCC magnesium hydrides Mg_7MH_{16} and Mg_6MH_{16} (M = Ti, V, Nb): An ab initio study. *Int. J. Hydrogen Energy* **2010**, *35*, 2025–2032. [CrossRef]
37. Dai, J.H.; Song, Y.; Yang, R. First Principles Study on Hydrogen Desorption from a Metal (=Al, Ti, Mn, Ni) Doped MgH_2 (110) Surface. *J. Phys. Chem. C* **2010**, *114*, 11328–11334. [CrossRef]
38. Kumar, M.; Kamal, R.; Thapa, R. Screening based approach and dehydrogenation kinetics for MgH_2: Guide to find suitable dopant using first-principles approach OPEN. *Sci. Rep.* **2017**, *7*, 15550. [CrossRef] [PubMed]
39. Van Mal, H.H.; Buschow, K.H.J.; Miedema, A.R. Hydrogen absorption in $LaNi_5$ and related compounds: Experimental observations and their explanation. *J. Less Common Met.* **1974**, *35*, 65–76. [CrossRef]
40. Lakhal, M.; Bhihi, M.; Benyoussef, A.; El Kenz, A.; Loulidi, M.; Naji, S. The hydrogen ab/desorption kinetic properties of doped magnesium hydride MgH_2 systems by first principles calculations and kinetic Monte Carlo simulations. *Int. J. Hydrogen Energy* **2015**, *40*, 6137–6144. [CrossRef]
41. Alapati, S.V.; Johnson, J.K.; Sholl, D.S. Identification of Destabilized Metal Hydrides for Hydrogen Storage Using First Principles Calculations. *J. Phys. Chem. B* **2006**, *110*, 8769–8776. [CrossRef] [PubMed]
42. Yu, R.; Lam, P.K. Electronic and structural properties of MgH2. *Phys. Rev. B* **1988**, *37*, 8730–8737. [CrossRef]
43. Westerwaal, R.J.; Broedersz, C.P.; Gremaud, R.; Slaman, M.; Borgschulte, A.; Lohstroh, W.; Tschersich, K.G.; Fleischhauer, H.P.; Dam, B.; Griessen, R. Study of the hydride forming process of in-situ grown MgH_2 thin films by activated reactive evaporation. *Thin Solid Films* **2008**, *516*, 4351–4359. [CrossRef]